Supplementary Material

Pore Structure Modulation and Defect Engineering of Soft Carbon@Coal-Derived Hard Carbon for Enhanced Sodium Storage Application in SIBs

Xinhui Jin[a], Haoyu Ma[a], Guoping Liu[c], Xikun Zhang[b], Dong Wang[a], Dejie Mo[a], Jiangyan Xie[a], Lirong Feng[a], Maochun Wu[c], Baolian Su[b], Xiaohui Guo[a*]

[a]Key Lab of Synthetic and Natural Functional Molecule Chemistry of Ministry of Education, The College of Chemistry and Materials Science, Northwest University, Xi'an 710069, China.

[b]Department of inorganic chemistry, University of Namur, 61 rue de Bruxelles, B-5000 Namur, Belgium.

[c]Department of Mechanical Engineering, The Hong Kong Polytechnic University, Kowloon, Hong Kong SAR, 999077, P. R. China

*Corresponding author Email: guoxh2009@nwu.edu.cn

Table of contents

Physical and chemical characterizations

The microstructure and morphology of the samples were analyzed by using a field emission scanning electron microscope (SEM, model Zeiss Sigma 300) and a transmission electron microscope (TEM, model JEM 2110 F). The surface area and pore structure of the as-synthesized samples were measured by the N_2 adsorption-desorption technique, which was conducted at 77 K by using an Tristar II 3020 surface area test system (American Mack Instrument Company). The values of the surface area were calculated via the Brunauer – Emmett – Teller (BET) model. The X-ray diffraction (XRD) patterns of the samples were collected by a D8 Advance X-ray diffractometer with Cu *Kα* radiation (λ = 1.540598 Å) at 40 kV and 40 mA. The in situ XRD measurements of electrodes were performed with a Panalytical Empyrean X-ray diffractometer with Cu Ka radiation. The surface chemical substances of the samples were detected by using a Thermo Scientific *Kα* X-ray photoelectron spectrometer (American Thermo Fisher Scientific Company) with an excitation source of monochromatic Al-*Kα* (1468.6 eV). FTIR spectra were recorded on an FTIR spectrometer 320 (Tensor27). Raman spectra were recorded with a TY2017003172 Raman instrument equipped with a 532 nm wavelength laser.

Electrochemical Measurements

CR2032 coin cells were used for all the electrochemical measurements. 80 wt.% of the HC samples, 10 wt.% of CMC as the binder and 10 wt.% of super P as the conductive carbon were mixed with distilled water to make the slurry, which was then coated onto Cu foils to make the electrodes. All the electrodes were dried in a vacuum oven at 100 °C overnight, and the active materials are kept at around 2–4 mg/cm^2. Half cells were assembled by using glass fibers as the separator, sodium metal as negative electrodes, the electrolyte was 1 M $NaPF_6$ in Diethylene glycol dimethyl ether (Diglyme). According to the normal button assembly sequence, the HC and the electrolyte, diaphragm, and sodium sheet were assembled in a glovebox filled with argon (H_2O, $O_2 < 1$ ppm). The galvanostatic charge and discharge testing was carried out on a BTSC CT-4008Tn battery test system at room temperature in the potential range of 0.01−3.0 V (relative to Na^+/Na). Cyclic voltammetry (CV) was conducted using a CHI700E electrochemical workstation with a sweep rate of 0.1~1 mV/s and a voltage range from 0.01 to 3.0 V (vs Na^+/Na). For in situ XRD measurements, the charge-discharge process was carried out at 0.03 A/g with a 2θ scan range of 10^o–50^o.

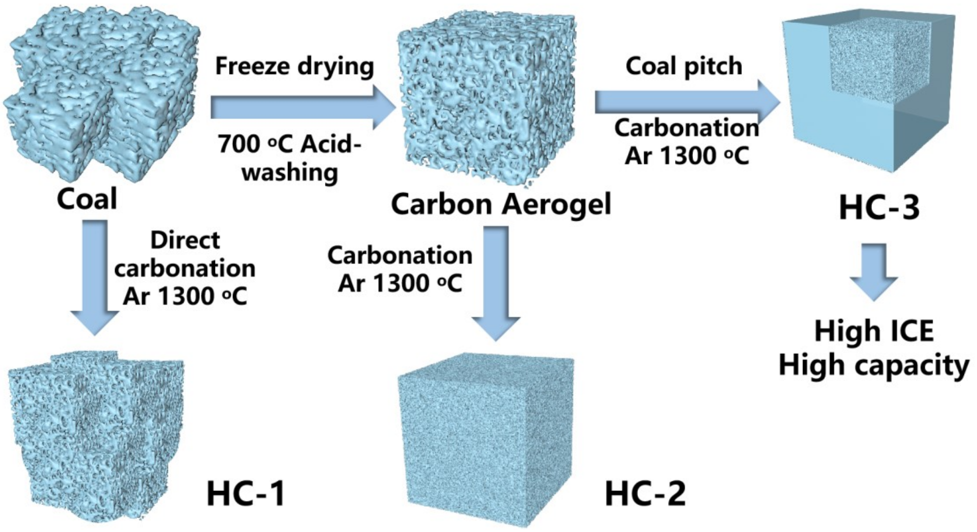

Figure S1. Schematic illustration of the synthesis process of HC-1, HC-2, and HC-3.

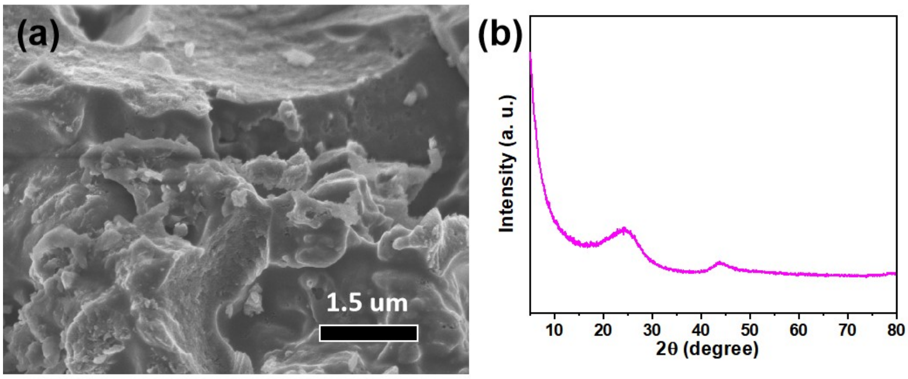

Figure S2. (a) SEM images, and (b) XRD patterns of HC-4.

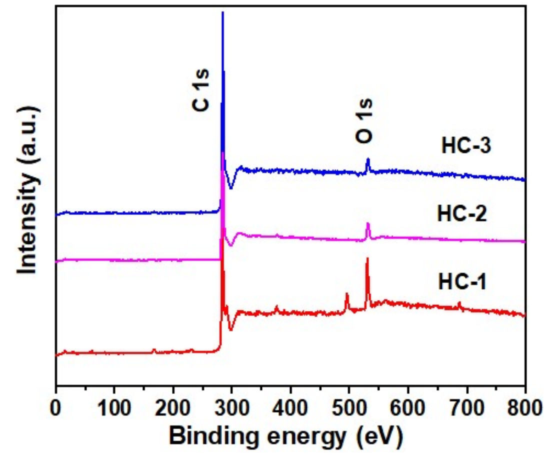

Figure S3. Full XPS survey spectra of HC-1, HC-2, and HC-3.

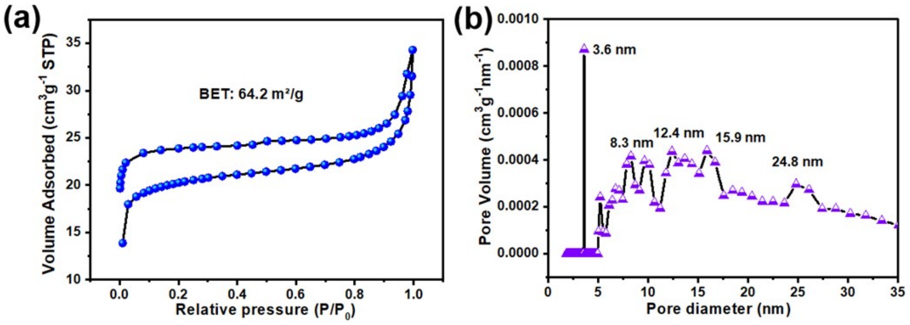

Figure S4. (a) Nitrogen adsorption/desorption isotherms and (b) pore diameter distribution of AC-700.

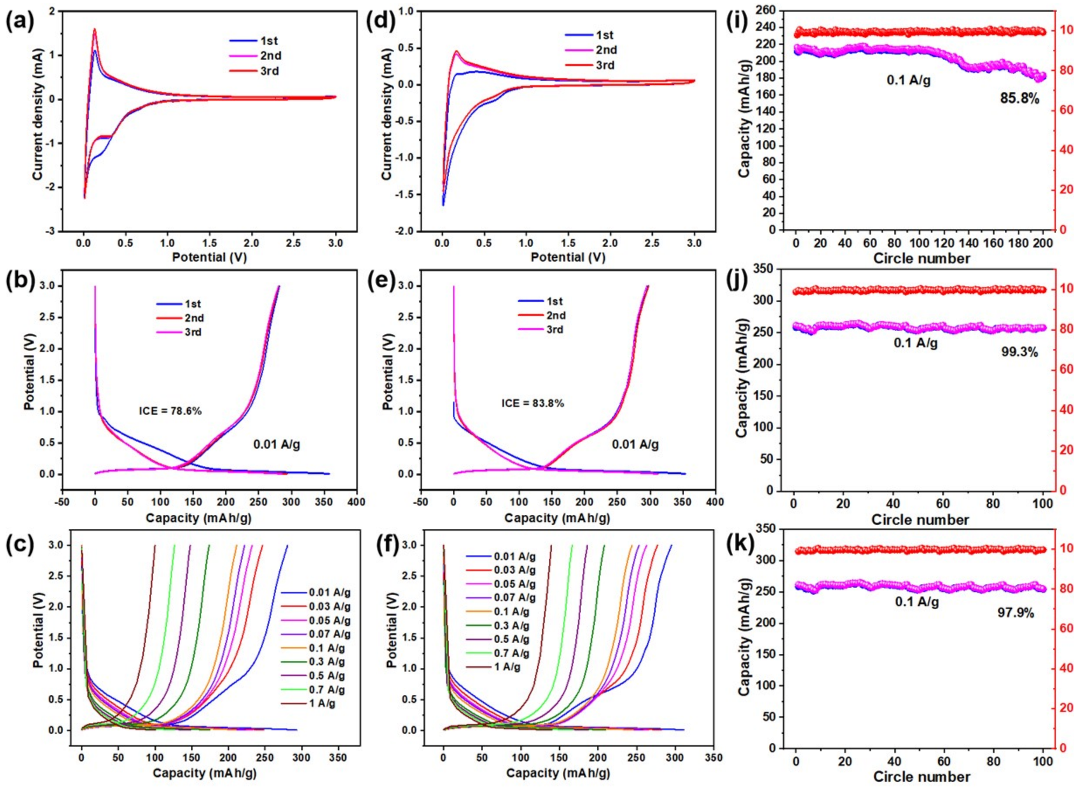

Figure S5. Initial three-cycle CV curves of (a) HC-1 and (d) HC-2 at 1 mV/s. Initial three-cycle GCD curves at 0.01 A/g of (b) HC-1 and (e) HC-2. The GCD curves of (c) HC-1 and (f) HC-2 electrodes at different current densities. Long cycling performances of (i) HC-1, (j) HC-2, and (k) HC-3 electrodes at the current density of 0.1 A/g for 100 cycles.

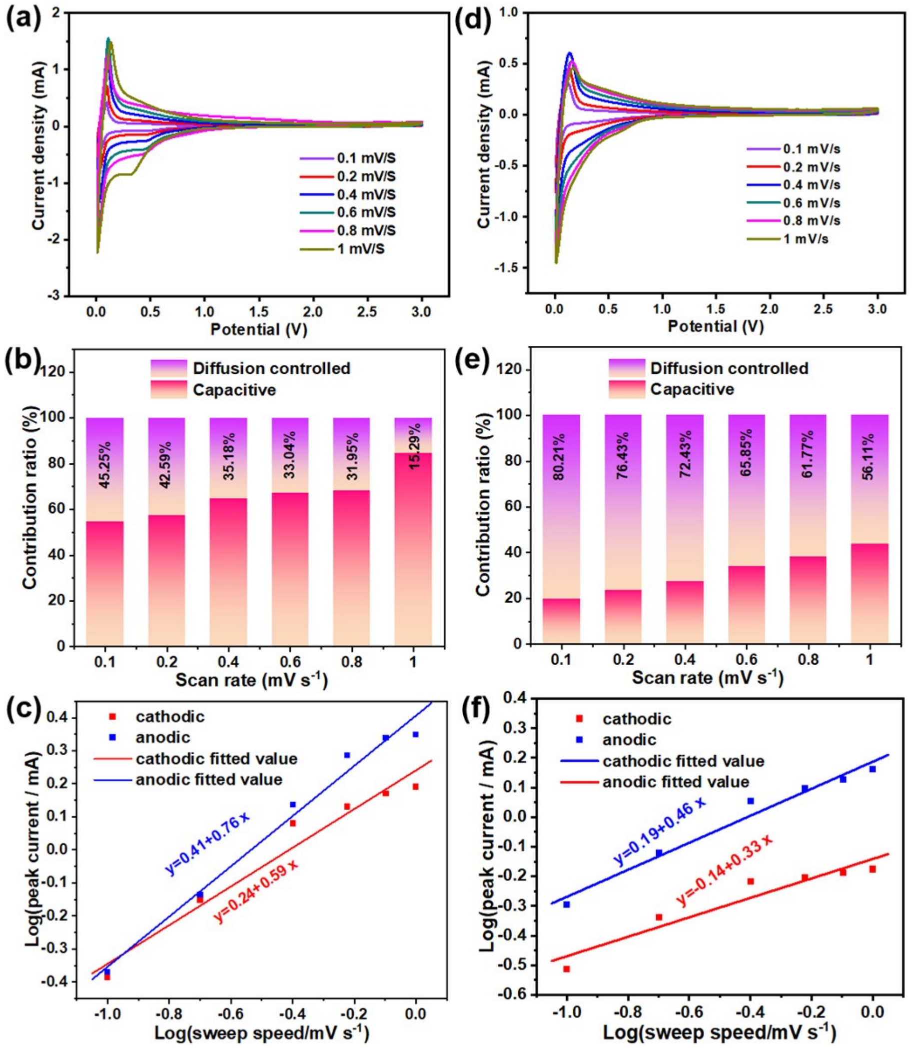

Figure S6. CV curves of (a) HC-1 and (b) HC-2 at different scan rates. Normalized contribution ratio of capacitive capacity at different scan rates for (b) HC-1 and (e) HC-2. Fitting plots of (c) HC-1 and (f) HC-2 for the oxidization peak and the reduction peak.

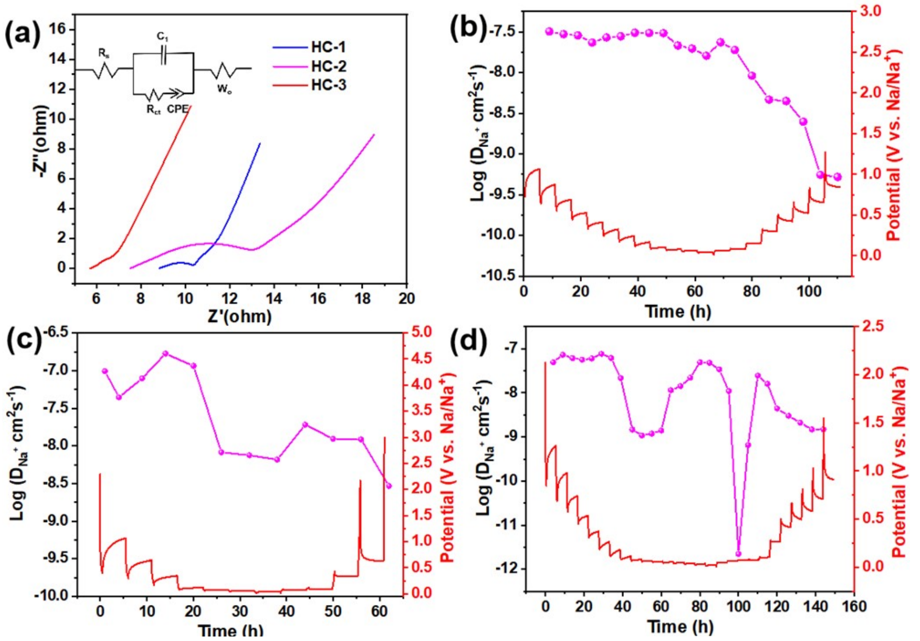

Figure S7. (a) Nyquist plots, (b-d) GITT profiles and calculated Na^+ diffusion coefficient during discharge and charge of HC-1, HC-2, and HC-3.

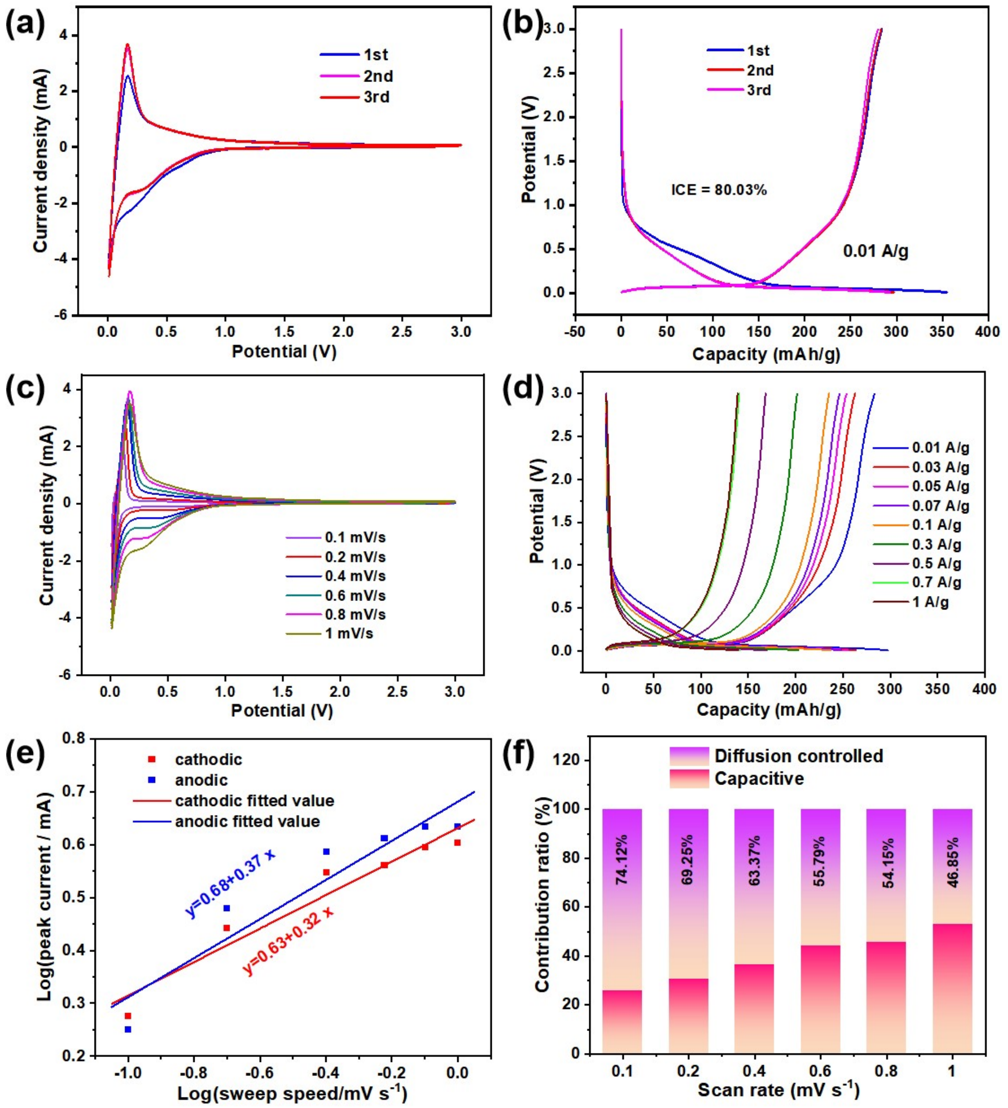

Figure S8. Initial three-cycle (a) CV curves at 1 mV/s and (b) GCD curves at 0.01 A/g, (c) CV curves at different scan rates and (d) GCD curves at different current densities, (e) relationship between the logarithm of cathodic peak current and logarithm of scan rates, and (f) normalized contribution ratio of capacitive capacity at different scan rates of HC-4.

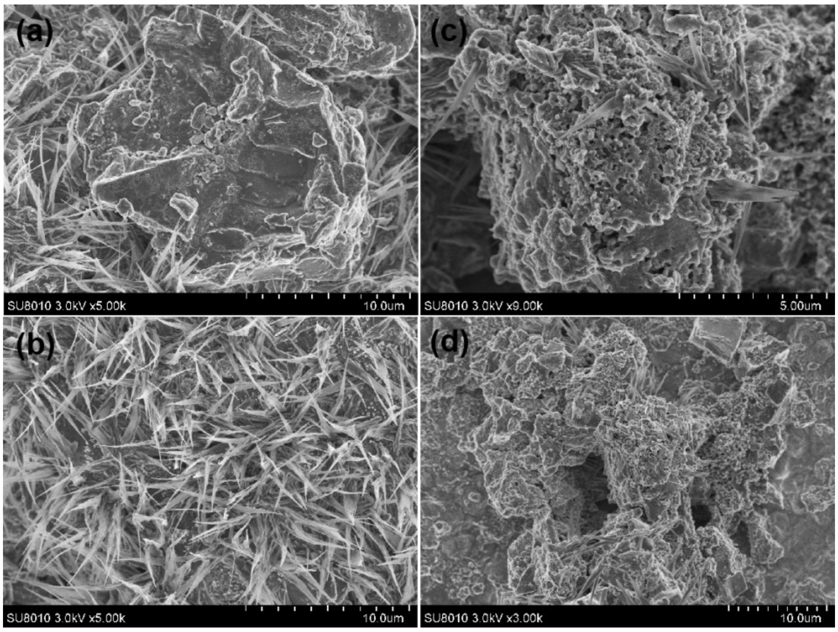

Figure S9. SEM images of (a,b) HC-2 and (c,d) HC-3 after long-term cycling.

Table S1. Physical parameters of HC-1, HC-2, HC-3 and HC-4 samples from XRD.

Sample	2θ (deg)	d_{002} (nm)	L_c (nm)	L_a (nm)	FWHM	τ
HC-1	23.44	0.375	1.55	6.02	0.5245	4.13
HC-2	23.49	0.38	1.48	4.59	0.5518	3.89
HC-3	24.59	0.378	1.61	6.39	0.5063	4.26
HC-4	24.49	0.37	1.56	6.82	0.5136	4.22

Table S2. Types and content of the C 1s and O 1s for HC-1, HC-2, and HC-3.

		HC-1		HC-2		HC-3	
C1s	C-Csp2	284.54	22.29%	284.55	15.69%	284.56	26.96%
	C-Csp3	284.85	21.12%	284.83	33.65%	284.83	30.67%
	C-O	285.34	17.84%	285.32	22.85%	285.42	20.32%
	C=O	285.7	31.07%	286.28	20.35%	286.3	19.97%
	COOR*	288.76	7.68%	289.15	7.46%	289.46	2.08%
O1s	C=O	530.48	12.40	530.74	5.56%	531	4.90%
	C-O	532.13	15.71	532.38	51.46%	532.04	62.43%
	COOR	533.77	36.89%	533.89	42.98%	533.9	32.67%

Table S3. Pore structural parameters of various carbon materials.

Sample	S_{BET} (m^2/g)	S_{mic} (m^2/g)	V_{total} (cm^3/g)	V_{mic} (cm^3/g)	V_{Mic}/V_{Total} (%)
HC-1	6.8	3.8	0.0083	0.0001	1.2
HC-2	35.5	16.0	0.0184	0.0129	70
HC-3	1.3	1.6	0.1119	0	0
AC-700	64.2	16.8	0.038	0.0322	84.6

Table S4. Electrochemical performance comparison of HC anodes synthesized from different raw materials with our HC anode material in SIBs.

	Raw Material	Carbonization	ICE	Specific Capacity (mAh/g)	Cycle stability	Ref.
HC	coal	1400	64.8%	303.1 (50 mA/g)	73.1% (300 cycles) (1000 mA/g)	S1
HC	coal	1300	82.3%	308.4 (30 mA/g)	85.1% (800 cycles) (90 mA/g)	S2
N-HC	coal	1200	~	282 (50 mA/g)	86.9% (500 cycles) (100 mA/g)	S3
HC	coal−pitch	1100	82.8%	300.83 (20 mA/g)	~75% (100 cycles) (20 mA/g)	S4
HC/SC	coal−tar pitch	1200	94.1%	293.3 (20 mA/g)	99% (100 cycles) (20 mA/g)	S5
HC	Subbituminous	1300	79.5%	291 (20 mA/g)	82% (200 cycles) (50 mA/g)	S6
HC	bituminous coal	1300	72.03%	313.5 (30 mA/g)	77.4% (500 cycles) (300 mA/g)	S7
N, S-HC	coal	1200	50.82%	314.2 (20 mA/g)	93.5% (200 cycles) (100 mA/g)	S8
HC	bituminous coal	1200	80.9%	246.8 (30 mA/g)	69.4% (200 cycles) (500 mA/g)	S9
HC/SC	anthracite	1300	85.9%	322 (10 mA/g)	87.1% (400 cycles) (1000 mA/g)	This work

References

[S1] R. Ma, Y. Chen, Q. Li, B. Zhang, F. Chen, C. Leng, D. Jia, N. Guo, L. Wang, Oxygen-driven closing pore formation in coal-based hard carbon for low-voltage rapid sodium storage, *Chem. Eng. J.,* 2024, **493,** 152389.

[S2] K. Wang, F. Sun, H. Wang, D. Wu, Y. Chao, J. Gao, G. Zhao, Altering Thermal Transformation Pathway to Create Closed Pores in Coal-Derived Hard Carbon and Boosting of Na^+ Plateau Storage for High-Performance Sodium-Ion Battery and Sodium-Ion Capacitor, *Adv. Funct. Mater.,* 2022, **32,** 2203725.

[S3] R. Li, B. Yang, A. Hu, B. Zhou, M. Liu, L. Yang, Z. Yan, Y. Fan, Y. Pan, J. Chen, T. Li, K. Li, J. Liu, J. Long, Heteroatom screening and microcrystal regulation of coal-derived hard carbon promises high-performance sodium-ion batteries, *Carbon*, 2023, **215,** 118489.

[S4] R. Xu, Z. Yi, M. Song, J. Chen, X. Wei, F. Su, L. Dai, G. Sun, F. Yang, L. Xie, C.-M. Chen, Boosting sodium storage performance of hard carbons by regulating oxygen functionalities of the cross-linked asphalt precursor, *Carbon*, 2023, **206**, 94-104.

[S5] X.X. He, J.H. Zhao, W.H. Lai, R. Li, Z. Yang, C.M. Xu, Y. Dai, Y. Gao, X.H. Liu, L. Li, G. Xu, Y. Qiao, S.L. Chou, M. Wu, Soft-Carbon-Coated, Free-Standing, Low-Defect, Hard-Carbon Anode To Achieve a 94% Initial Coulombic Efficiency for Sodium-Ion Batteries, *ACS Appl. Mater. Interfaces,* 2021, **13,** 44358-44368.

[S6] H. Lu, S. Sun, L. Xiao, J. Qian, X. Ai, H. Yang, A.-H. Lu, Y. Cao, High-Capacity Hard Carbon Pyrolyzed from Subbituminous Coal as Anode for Sodium-Ion Batteries, *ACS Appl. Energy Mater.,* 2019, **2**, 729-735.

[S7] Y. Zhu, X. Tang, Z. Kong, Z. You, Y. Zhang, Y. Duan, Y. Zhang, Pre-oxidation modification of bituminous coal-based hard carbon for high-quality sodium ion storage, *Solid State Ionics*, 2024, **416,** 116668.

[S8] H.-z. Niu, H.-h. Wang, L.-y. Sun, C.-r. Yang, Y. Wang, R. Cao, C.-g. Yang, J. Wang, K.-w. Shu, N, S co-doped coal-based hard carbon prepared by two-step carbonization and a molten salt template method for sodium storage, *New Carbon Materials*, 2024, **39**, 297-307.

[S9] Z. Lou, H. Wang, D. Wu, F. Sun, J. Gao, X. Lai, G. Zhao, Microcrystalline regulation of bituminous coal derived hard carbon by pre-oxidation strategy for improved sodium-ion storage, *Fuel*, 2022, **310,** 122072.